IEEE Access
Multidisciplinary ⋮ Rapid Review ⋮ Open Access Journal

Received 4 May 2023, accepted 20 June 2023, date of publication 26 June 2023, date of current version 5 July 2023.

Digital Object Identifier 10.1109/ACCESS.2023.3289709

RESEARCH ARTICLE

Motor Imagery Decoding Enhancement Based on Hybrid EEG-fNIRS Signals

TAO XU[1], ZHENGKANG ZHOU[1], YULIANG YANG[1], YU LI[1], JUNHUA LI[1,2], (Senior Member, IEEE), ANASTASIOS BEZERIANOS[3], (Senior Member, IEEE), AND HONGTAO WANG[1], (Senior Member, IEEE)

[1]Faculty of Intelligent Manufacturing, Wuyi University, Jiangmen 529000, China
[2]School of Computer Science and Electronic Engineering, University of Essex, CO4 3SQ Colchester, U.K.
[3]Centre for Research and Technology Hellas (CERTH), Hellenic Institute of Transport (HIT), 54627 Thessaloniki, Greece

Corresponding author: Hongtao Wang (nushongtaowang@qq.com)

This work was supported in part by the Special Projects in Key Fields Supported by the Technology Development Project of Guangdong Province under Grant 2020ZDZX3018, in part by the Special Fund for Science and Technology of Guangdong Province under Grant 2020182, in part by the Wuyi University and Hong Kong & Macao Joint Research and Development Project 2019WGALH16, in part by the Startup Funds for Scientific Research of High-Level Talents of Wuyi University under Grant 2019AL020, and in part by the Projects for International Scientific and Technological Cooperation under Grant 2023A050507068.

This work involved human subjects or animals in its research. Approval of all ethical and experimental procedures and protocols was granted by the Institutional Review Committee of Jiangmen Central Hospital under Application No. [2021] No.8 A, and performed in line with the Study of EEG-fNIRS Dynamic Brain Functional Connectivity.

ABSTRACT This study explores the combination of electroencephalogram (EEG) and functional near-infrared spectroscopy (fNIRS) to enhance the decoding performance of motor imagery (MI) tasks for brain-computer interface (BCI). The experiment involved measuring 64 channels of EEG signals and 20 channels of fNIRS signals simultaneously during a task of the left-right hand MI. By combining these two types of signals, the study aimed to understand how feature fusion affected classification accuracy for MI. The EEG signals were filtered into three bands (θ: 4-7 Hz, α: 8-13 Hz, β: 14-30 Hz), while the fNIRS signals were filtered into 0.02-0.08 Hz to improve signal quality for subsequent analysis. The common spatial patterns (CSP) algorithm was utilized to extract features from both EEG and fNIRS signals. This allowed the researchers to create a fused signal with both EEG and fNIRS features that could then be processed using principal component analysis (PCA). Finally, the processed data was fed into a support vector machine (SVM) classifier, which improved the mean accuracy rate of MI to 92.25%. By comparing the classification accuracies obtained with fused and unfused segments of EEG and fNIRS signals, the study discovered that fusing the signals significantly improved classification accuracy by 5%-10%. Furthermore, analyzing the activated brain regions using fNIRS showed that the auxiliary motor cortex was significantly activated during MI. These results demonstrate that hybrid signals with a fusion strategy can enhance the stability and fault tolerance in BCI systems, making them valuable for practical applications.

INDEX TERMS Motor imagery, functional near-infrared spectroscopy, common spatial pattern, principal components analysis, brain–computer interface.

I. INTRODUCTION

MI is a cognitive task that involves mentally imagining oneself performing a physical movement without actually moving. Combining MI with physical exercise has been shown to be beneficial for learning new skills and improving sports performance [1]. Additionally, neuroscience research has used MI as a paradigm to investigate brain activity prior to the execution of action [2], [3]. MI-based brain-computer interfaces (BCIs) have potential applications in restoring motor movements for individuals who are paralyzed, disabled, or have suffered a stroke [4], [5]. By utilizing MI to control external devices, such as robotic arms or computer cursors, individuals with motor disabilities can bypass their

The associate editor coordinating the review of this manuscript and approving it for publication was Jason Gu.

impaired neuromuscular system and interact with the world around them in new ways. This could greatly improve their quality of life and independence.

To create a BCI that is based on measuring MI, EEG signals are commonly used to record the activity of cortical neurons using scalp electrodes. This method has several advantages, including its non-invasiveness, portability, and ability for long-term monitoring. [6], [7], [8]. Additionally, EEG signals provide high temporal resolution, allowing for real-time measurement of MI which can be converted into control signals to assist with motor movements [6], [9], [10]. However, a single modal assessment of EEG induces some disadvantages such as the non-intuitive representation of brain activity and low spatial resolution. It is also extensively reported that better BCI performance can be achieved with multimodal analysis instead of standalone EEG signals [11], [12], [13], [14], [15]. On this basis, multimodal studies which assess both brain's electrical activity and hemodynamic activity attract much interest. Hemodynamic activity can be recorded by position emission tomography (PET), functional magnetic resonance imaging (fMRI), and fNIRS, whereas only fMRI and fNIRS can simultaneously do the recording with EEG devices. Despite the availability of multiple recording modalities, the combination of EEG-fNIRS is emerging as a promising approach due to its low cost, portability, less discomfort, low interference, and good spatio-temporal resolution [16], [17], [18].

However, simply measuring these signals isn't enough - we also need to extract useful information from them in order to train our machine learning algorithms to recognize specific patterns of brain activity. Different researchers have used different methods for doing this. For example, Fazli et al. recorded event-related desynchronizations (ERDs) and time average fNIRS concentration changes during MI whereas Ma et al. adopted EEG power spectral densities and fNIRS signals amplitudes [12], [19]. In addition, the peak amplitude of EEG and the mean values of oxygenated hemoglobins (HbO) and deoxygenated hemoglobins (Hb) for fNIRS can also be applied as the input to a linear discriminant analysis (LDA) classifier [15]. Based on the aforementioned fused features, although the MI classification accuracy or the movement recognition accuracy can range between 65%-95%, which is higher than the results derived from standalone EEG or fNIRS features, feature extraction should be specified into different segmentation in the time domain or frequency bands in the frequency domain. For standalone EEG-based BCI, the CSP algorithm is widely used for extracting spatial features by constructing spatial filters for differentiating various kinds of MI. However, searching for the best spatial filter still depends on the information in the temporal domain, which makes it to be sensitive to temporal noise [20]. Although a series of methods such as common spatial spectrum pattern (CSSP) or common sparse spectral spatial pattern (CSSSP) were proposed, a bandpass filter that confines the signal in a certain band can largely improve the effect of a CSP algorithm [21], [22]. In this way, filter bank common spatial pattern (FBCSP) with its variants was proposed, which can extract features in different bands simultaneously [20], [23], [24], [25], [26].

In this study, we collected fNIRS and EEG signals of MI of 15 healthy subjects at the same time. A new EEG fNIRS multi-mode MI decoding method is implemented: the CSP algorithm is used to extract two single-mode features respectively, and PCA reconstructs the fused features into a new set of features. Then support vector machine (SVM) is used as a classifier to compare the classification effect before and after feature fusion. In addition, we use NIRS statistical parametric mapping (SPM) to generate brain-activated images based on the MI contrast of left and right-hand. The rest of the paper is organized as follows: Section II explains the methods we used, including information about the subjects, data collection, experimental protocol, and data processing and analysis. In Section III, we present the experimental results, and in Section IV, we discuss these results. Finally, we provide a conclusion in Section V.

II. METHODS

A. SUBJECTS

In this research, we used two datasets. The first dataset, which we collected ourselves, consisted of twenty healthy individuals from Wuyi University. There were 5 males and 15 females with an average age of 21.5 years old. All participants confirmed that they did not have any chronic physical or mental illnesses. Before the experiment began, we asked the participants to avoid consuming caffeine or alcohol for four hours prior to the recording and to refrain from any strenuous exercise. They also had to sign an informed consent form and declare that they had never participated in an EEG experiment before. The Institutional Review Committee of Jiangmen Central Hospital approved this study. The second dataset, Dataset B, is a collection of public EEG-fNIRS data sets [27]. It included 29 healthy subjects, 14 males and 15 females, with an average age of 28.5 years old. Twenty-eight of these subjects were right-handed, and one was left-handed.

B. EXPERIMENTAL PROTOCOL

In this experiment, we used a measuring cap that included a 64-channel EEG system (SynAmps2 from Neuroscan in El Paso, Texas, USA), as well as a 20-channel fNIRS acquisition system called OXYMON MK III from Artinis in Nijmegen, Netherlands (Figure 1A). The EEG acquisition system is composed of 64 unipolar, 4 bipolar, and 2 high-level inputs, with a total of 70 leads, whose sampling rate of each lead is adapted to 1000 Hz in this experiment (Figure 1B) whereas the fNIRS which emits two wavelengths of 762.0 nm and 845.5 nm with a sampling rate of 50 Hz. Two Intel (R) core (TM) i5-7200u duo 2.7 GHz hosts (Vostro 3710 from Dell, Texas, USA) are used to run fNIRS and EEG acquisition systems, respectively.

Figure 1B and Figure 1C depict the arrangement of EEG electrodes and fNIRS sources and detectors. Prior to recording, we ensured that the impedance between the skin and

electrodes was below 20 kΩ, and that the intensity of light reception for fNIRS was above 200. Participants were seated comfortably in a chair with their hands resting naturally on their thighs. They were then instructed to perform a hand motor imagery task based on random image stimuli, which involved alternating between a 16-second rest state and an 8-second task state. (Figure 1D). The peak response of fNIRS signals appears about 8 seconds after the stimulation onset under the influence of hemodynamics [28]. Subjects were asked to imagine corresponding hand movements based on the images on the display. The image task was randomly provided with a total of 50 left-hand experiments and 50 right-hand experiments. In terms of dataset B, the experimental procedure is similar to ours whereas the distribution of electrodes is different (Figure 1C) and a 2-second visual guidance is added for each trial of MI (Figure 1E). For more details, please refer to [27].

C. MULTIMODAL SIGNAL PROCESSING FOR MI CLASSIFICATION

To achieve high accuracy of MI classification, multimodal fused signals are processed following four steps:

Step 1: signal preprocessing

As MI feature representations are embedded by different frequency bands of EEG signals (θ: 4-7 Hz, α: 8-13 Hz, β: 14-30 Hz), sixth-order Butterworth band-pass filters worked as filter bank (FB) were carried out for filtering EEG signals into different bands A control group was also proposed in which the EEG signals were filtered into 4-30 Hz. Furthermore, fNIRS signals were also filtered by a sixth-order Butterworth band-pass filter. Currently, the filtering of fNIRS use different high pass filter or low pass [29], [30]. If bandpass filtering is chosen, the filtering range will be selected based on the required noise frequency reduction and different task frequencies [31], [32], [33], [34]. Considering that the task frequencies of our two datasets are 0.04 Hz (1/24) and 0.03 Hz (1/27-1/29), we have chosen 0.02 Hz-0.08 Hz bandpass filtering.

Step 2: CSP feature extraction algorithm

The CSP algorithm [35] was used to extract features from multi-channel binary classification tasks. The principle of the CSP algorithm is to maximize the covariance difference between two types of data to achieve high discrimination features. In this experiment, EEG signals were collected from 64 channels whereas fNIRS signals were collected from 20 channels. Suppose a group of data with one hand is the matrix, where i is the label for a certain hand (i = 1 means left-hand, i = 2 means right-hand), j means the group number, and the total number of groups on the left-hand and right-hand is n (j ⩽ n). Then the covariance matrix corresponding to a single group of stimuli is calculated as follows [21]:

$$A_j^i = \frac{D_j^i \left(D_j^i\right)^T}{trace\left(D_j^i \left(D_j^i\right)^T\right)}. \tag{1}$$

Then the covariance matrix of the overall data is the sum of the average values of all single-group stimulus covariance matrices of the two data types. Assuming that $\overline{A_l}$ is the average of the left-hand covariance and $\overline{A_r}$ is the average of the right-hand covariance. after calculating the covariance matrix of overall data, it is necessary to decompose $\overline{A_{all}}$ by eigenvalue, which is calculated as follows [36]:

$$\overline{A_{all}} = PBP^T, \tag{2}$$

where matrix B is a diagonal matrix composed of $\overline{A_{all}}$ eigenvalues and matrix P is the eigenvector corresponding to matrix B. The eigenvalues are then arranged into descending order, and a whitening matrix F is calculated as follows [35]:

$$F = (B)^{-\frac{1}{2}} P^T \tag{3}$$

After obtaining the whitening matrix, the spatial filter will be constructed. The whitening matrix F is used to process the average value G_l of the left-hand data covariance and the average value G_r of the right-hand data covariance, respectively as follows [36]:

$$G_l = F\overline{A_l}F^T, \quad G_r = F\overline{A_r}F^T. \tag{4}$$

By decomposing G_l and G_r, we can get:

$$G_l = \Gamma\alpha_l\Gamma^T, \quad G_r = \Gamma\alpha_r\Gamma^T, \tag{5}$$

where Γ Is the eigenvector, α_l and α_r are the eigenvalues of G_l and G_r, respectively, and the summation of which is equal to the identity matrix $E = \alpha_l + \alpha_r$. Therefore, when the eigenvalue of G_l reaches the maximum, its corresponding eigenvector Γ will minimize the eigenvalue α_r of G_r, when the eigenvalue of G_l reaches the minimize, its corresponding eigenvector Γ will maximize the eigenvalue α_r of G_r. Thus, the rule can project the two types of signals to different regions as much as possible for the initial classification purpose. Finally, the corresponding projection matrix H can be represented as follows [35]:

$$H = P^T F. \tag{6}$$

The filtered matrix $\Omega_{2m\times t}$ can be obtained from the original data $D_{ch\times t}$ through the spatial filter H, which is calculated as follows [21]:

$$\Omega_{2m\times t} = H_{2m\times ch} D_{ch\times t}. \tag{7}$$

At this time, the matrix $\Omega_{2m\times t}$ is the result of $D_{ch\times t}$ filtering. Finally, $\Omega_{2m\times t}$ is calculated as follows [21]:

$$\xi_j = log\left(\frac{var\left(\Omega_j\right)}{\sum_{j=1}^{2m} var\left(\Omega_j\right)}\right), \quad j = 1, 2, \ldots, 2m, \tag{8}$$

where $var\left(\Omega_j\right)$ is the variance of row j in $\Omega_{2m\times t}$. ξ_j is the feature vector we want to extract. In this paper, we choose four pairs as the number of features [37].

Step 3: feature fusion

After data preprocessing, signals in frequency band 4∼30 Hz or separated three frequency bands of 4-7 Hz,

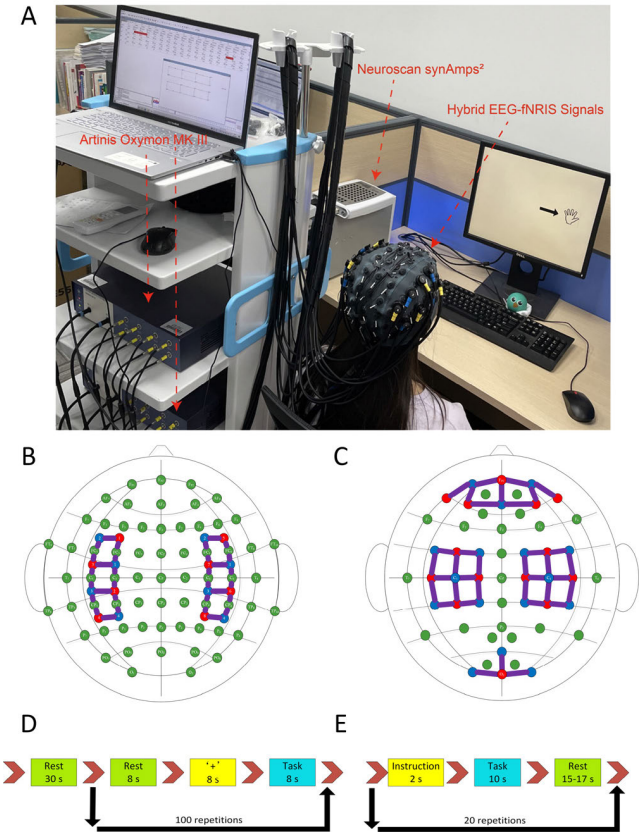

FIGURE 1. Experimental setup for dataset A and dataset B. A, experiment setup. B, fNIRS and EEG electrode distribution for dataset A. C, fNIRS and EEG electrode distribution for dataset B, red and blue dots represent near-infrared optobes sources and detectors respectively, and green dots represent EEG electrodes, purple is the channel formed by near-infrared optobes sources and detectors electrodes. D, flow chart of experimental paradigm for dataset A. E, flow chart of experimental paradigm for dataset B.

8-13 Hz, and14-30 Hz are obtained. The CSP is used to extract features of these two types of signals, and 8 features are extracted from each data band. Therefore, 8 and 24 features are obtained from data preprocessing, respectively. Due to fNIRS being divided into HbO and Hb signals, 8 features of each signal are extracted by the CSP. This means that 24 (8 plus16) or 40 (24 plus16) features are obtained after the fusion of EEG and fNIRS features.

Step 4: PCA feature selection and SVM classifier

In this paper, PCA recombines the original feature matrix ξ_{ij} obtained from CSP into a new set of unrelated comprehensive feature matrices. Select a set of unit orthogonal bases P, so that after the original feature is transformed to this set of bases, the covariance between two fields is 0, while the variance of the field is as large as possible. The covariance matrix C can be calculated by the following formula [38]:

$$C = \frac{1}{m}\xi_{ij}\xi_{ij}^{T}, \tag{9}$$

where C is also a symmetric matrix. ξ_{ij} gets the matrix Y after the base transformation of P, that is, $Y = PX$. Assuming that the covariance matrix of Y is D, the relationship between

TABLE 1. Data and methods used for MI classification.

	Filter	Feature extraction with CSP	Feature fusion	PCA	FB	SVM
EEG	4-30 Hz	√	N.A.	N.A.	N.A.	√
	4~7 Hz, 8~13 Hz and 14~30 Hz	√	N.A.	N.A.	√	√
fNIRS	0.02-0.08 Hz	√	N.A.	N.A.	N.A.	√
EEG + fNIRS	EEG: 4-30 Hz fNIRS: 0.02-0.08 Hz	√	√	N.A.	N.A.	√
	EEG: 4-30 Hz fNIRS: 0.02-0.08 Hz	√	√	√	N.A.	√
	EEG: 4~7 Hz, 8~13 Hz and 14~30 Hz fNIRS: 0.02-0.08 Hz	√	√	√	√	√

D and C is:

$$D = \frac{1}{m}YY^{T} = \frac{1}{m}(PX)(PX)^{T} = PCP^{T}. \tag{10}$$

Next, we diagonalize the covariance matrix C and arrange the diagonal elements from big to small, then the first K lines of P are the basis to be searched, where K is the dimension of the new irrelevant comprehensive eigenmatrix. According to the properties of a real symmetric matrix with n rows and n columns can be found n unit orthogonal eigenvectors, assuming that these n eigenvectors are $e_1, e_2, \ldots, e_n$. Then a matrix L can be found $L = (e_1 e_2 \ldots e_n)$, orthogonal basis $P = L^{T}$, new uncorrelated comprehensive characteristic matrix [38]:

$$Y = P\xi_{ij}. \tag{11}$$

The new feature group is linearly uncorrelated, so in theory, it will produce good classification results. The principal component score is the cumulative contribution rate obtained through covariance. Our approach for generating a feature subset involves several steps. First, we identify the principal component with the highest score and retain it as a feature. Then, we add the principal component with the next highest score to our feature set and continue this process until we've included all of the principal components.

Once we have selected our subset of PCA features, we pass them to an SVM classifier [39] for classification. To ensure the accuracy of the classifier, we use tenfold cross-validation. We terminate the process when we find the feature subset that yields the highest classification accuracy. Data and methods used for MI classification comparison are shown in Table 1.

D. BRAIN ACTIVATION

The activation results of brain regions in this experiment were obtained using NIRS SPM (KAIST bioimaging signal processing laboratory in daejeon, south korea). It uses the modified bill lambert law (MBLL) based on the generalized

linear model (GLM) [40]:

$$od = \varepsilon C \cdot DPF \cdot d + G, \tag{12}$$

optical density (od) refers to how much light is blocked or weakened as it passes through a substance. The amount of attenuation is affected by the absorption coefficient ε, the concentration of the substance (C), the differential path length factor (DPF), the linear distance between the fNIRS light source and detector (d), and an unknown factor (G) that accounts for the influence of brain tissue on near-infrared light absorption, scattering, and the shape of the light propagation path. To eliminate this unknown factor, we calculate the starting and ending concentrations of the substance and then subtract them from each other. This gives us the changes in both substance concentration and light attenuation, which we can express as $\Delta\ od$:

$$\Delta od = \varepsilon \Delta C \cdot DPF \cdot d, \tag{13}$$

the near-infrared light with HbO and Hb contents can be obtained at the incident wavelength λ_1 and reflection wavelength λ_2, respectively [40]:

$$\begin{cases} \Delta od_{\lambda_1} = \varepsilon^{\lambda_1}_{HbO} \Delta\,[HbO]\, DPFd + \varepsilon^{\lambda_1}_{Hb} \Delta\,[Hb] \cdot DPF \cdot d \\ \Delta od_{\lambda_2} = \varepsilon^{\lambda_2}_{HbO} \Delta\,[HbO]\, DPFd + \varepsilon^{\lambda_2}_{Hb} \Delta\,[Hb] \cdot DPF \cdot d, \end{cases} \tag{14}$$

where Δod_{λ_1} is the attenuation of light with an incident wavelength of λ_1, Δod_{λ_2} is the attenuation of light with a reflection wavelength of λ_2, and $\varepsilon^{\lambda_x}_{HbX}$ is the absorption coefficient of HbO or Hb at the corresponding wavelength. Further calculation can be obtained from [40]:

$$\begin{cases} \Delta\,[HbO] = \dfrac{\varepsilon^{\lambda_2}_{HbO} \Delta od_{\lambda_1} - \varepsilon^{\lambda_1}_{Hb} \Delta od_{\lambda_2}}{DPF \cdot d(\varepsilon^{\lambda_1}_{HbO} \varepsilon^{\lambda_2}_{Hb} - \varepsilon^{\lambda_2}_{HbO} \varepsilon^{\lambda_1}_{Hb})} \\ \Delta\,[Hb] = \dfrac{\varepsilon^{\lambda_1}_{HbO} \Delta od_{\lambda_2} - \varepsilon^{\lambda_2}_{Hb} \Delta od_{\lambda_1}}{DPF \cdot d(\varepsilon^{\lambda_1}_{HbO} \varepsilon^{\lambda_2}_{Hb} - \varepsilon^{\lambda_2}_{HbO} \varepsilon^{\lambda_1}_{Hb})}, \end{cases} \tag{15}$$

where $\Delta\,[HbX]$ is the change in HbO or Hb concentration.

By setting a comparison matrix, the activation area of the left brain relative to the right brain can be obtained, while the activation area of the right brain equivalent to the left brain can be obtained.

III. EXPERIMENTAL RESULT

There is a clear relationship between the number of features selected in PCA and the corresponding principal component value (Figure 2). Specifically, as the number of selected principal components increases, the amount of information retained from the original feature group also increases.

In terms of the statistics on the number of principal components selected by 20 subjects (Figure 3), we can observe that only a small percentage of subjects had principal components in the range of 1-10 or 31-40. This indicates that either too few or too many principal components may not be ideal for capturing the relevant information from the original feature group.

Interestingly, a significant proportion of subjects, 65%, had principal components in the range of 11-20. This suggests that this range of principal components may be optimal for retaining the relevant information while also reducing the dimensionality of the feature space.

Overall, these findings highlight the importance of carefully selecting the number of principal components in PCA to ensure that the relevant information is retained while avoiding overfitting or underfitting the data.

To verify the effectiveness of our PCA feature selection, we used SVM and KNN [42] classifiers to compare the classification accuracy before and after PCA (Figure 4). It can be seen that in the KNN classifier, the average classification accuracy after PCA (89.50 ± 7.1%) is higher than the average classification accuracy of simple fusion (61.00 ± 19.6%), and the average classification accuracy of FB-PCA (91.85 ± 4.2%) is higher than the average classification accuracy of PCA.

To illustrate the effectiveness of the hybrid feature to MI decoding, we compare the classification accuracy with separated EEG signals, fNIRS signals and the PCA (Figure 5). Bandpass filters with 4-30 Hz and 0.02-0.08 Hz are exerted on EEG signals and fNIRS signals respectively and the fused feature is also processed with such two filters. It can be seen that after feature fusion, the mean classification accuracy of MI for all subjects with multimodal EEG-fNIRS (88.00 ± 6.16%) is significantly higher than that with independent EEG signals (76.00 ± 8.46%) or independent fNIRS signals (71.25 ± 8.56%).

To show the capability of FB and PCA in EEG data preprocessing for MI decoding, we compare the mean classification accuracy with three fusion methods (Figure 5). To extract more subtle features within EEG signals, three bandpass filters (4-7 Hz, 8-13 Hz, 14-30 Hz) are applied respectively for EEG signals. It can be seen that the mean classification accuracy with the FB-PCA method for all subjects (92. 25 ± 4.99%) is significantly higher than that with the mere PCA method (88.00 ± 6.16%) and simple fusion method (55.25 ± 16.69%).

To verify the generalization of the preprocessing method, we use the same method to process both EEG and fNIRS signals in dataset B [27]. We compare the classification accuracy of MI decoding with separated EEG signals, fNIRS signals and a hybrid one deriving from dataset B (Figure 5). It can be seen that after feature fusion, the mean classification accuracy of MI for all subjects with multimodal EEG-fNIRS (96.90 ± 1.59%) is significantly higher than that with separated EEG signals (92.24 ± 1.90%) or fNIRS signals (53.56 ± 10.59%). Furthermore, the classification accuracy can also be improved by adding FB and PCA in data preprocessing for dataset B which is also shown in Figure 5. To better compare the classification effects of the single mode and the three fusion methods, we calculated the F1-score of the five classification methods. The experimental results are shown in Table 2. It can be seen that the F1-score of FB-PCA (73.96%) is significantly higher than that of single mode and the other two fusion

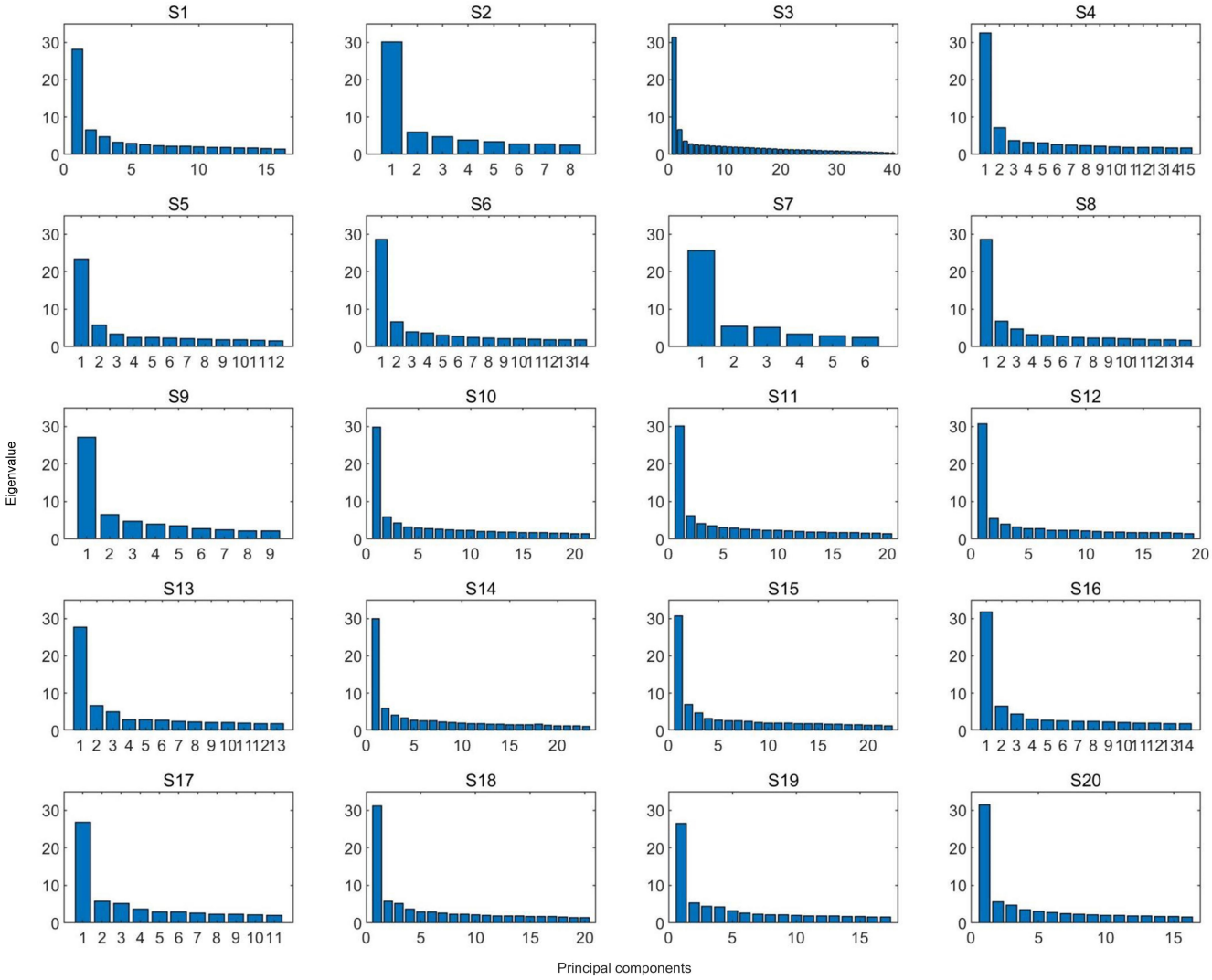

FIGURE 2. The relationship between the characteristic values of the subjects and the final selected principal component score, with the x-axis representing the number of principal components selected and their corresponding numbers, and the y-axis representing the corresponding characteristic values.

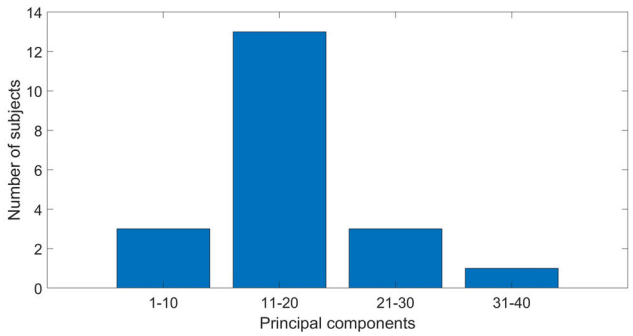

FIGURE 3. Distribution map of the number of principal components of subjects.

methods, and PCA (73.24%) is also higher than the F1-score of simple fusion (32.63%).

To further support our classification results, we use fNIRS signals from dataset A (Figure 6A) and dataset B (Figure 6B) to study the activation of brain regions during MI. The active areas of MI with dataset A are channels 12, 17 and 18 (right premotor cortex and supplementary motor cortex, primary motor cortex) with MI of the left hand (left figure). In contrast, the right side figure shows that channels 2, 3 and 8 (left premotor and supplementary motor cortex, dorsolateral prefrontal cortex) are activated by right-hand MI. However, although the left-right hand MI is activated by the contralateral brain region, the subregion of left-right hand MI is different for the two datasets. For dataset B, the left side figure shows that channels 13, 16, 18 (right dorsolateral prefrontal cortex, primary motor cortex, premotor and supplementary motor cortex of the right brain) are activated by the left-hand MI, and the right side figure shows that channel 1, 2, 4, 5 (left dorsolateral prefrontal cortex,

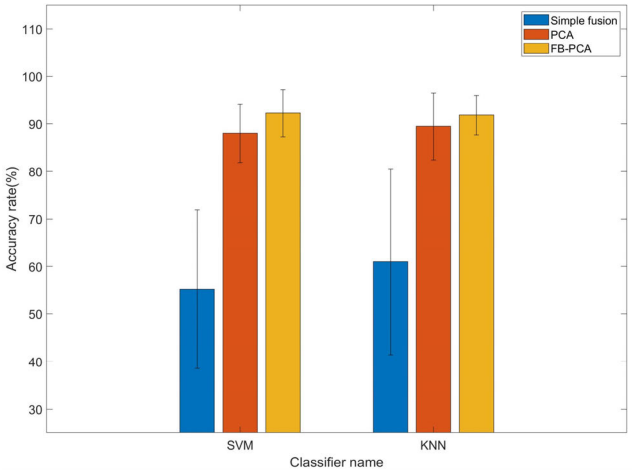

FIGURE 4. The average classification accuracy of PCA selected features in SVM and KNN classifiers.

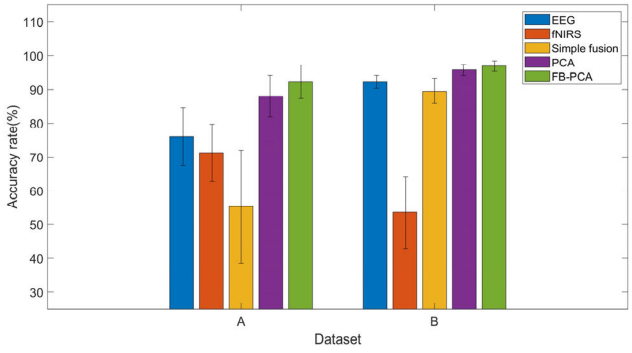

FIGURE 5. Classification accuracy of EEG, fNIRS, EEG, Original, PCA and FB-PCA and Hybrid in dataset A and dataset B.

the premotor and supplementary motor cortex of the left brain) are activated by the right hand MI. The results showed that there were significant differences in the activated brain regions when the subjects imagined the left- and right-hand movements.

The experimental results of this study are consistent with the existing research results on MI [43]. The auxiliary motor areas remain activated throughout the process of motor imagination, while the left and right brain areas are asymmetric, which may be related to the asymmetry of the brain [44].

IV. DISCUSSION

This study examined how the brain reacts when performing left-right hand motor imagery, using both EEG and fNIRS data to measure cortical activation. The researchers collected both types of signals at the same time, as simultaneous multimodal recording of brain activity has become increasingly popular in recent years, given that different recording methods reveal various mechanisms of brain function. [12], [14], [37]. For instance, EEG signals reflect assembled neural electrophysiology, so they have a high temporal resolution, as the firing rate of a neuron's burst state can exceed 200 Hz.

TABLE 2. Average accuracy and standard deviation before and after feature fusion AND F1-SCORE.

	Average accuracy rate (%) across subjects of dataset A	Average accuracy rate (%) across subjects of dataset B	F1-score (%)
EEG	76.00±8.46	92.24±1.90	54.08
fNIRS	71.25±8.56	53.56±10.59	46.96
CSP EEG: 4-30 Hz fNIRS: 0.02-0.08 Hz	55.25±16.69	89.48±3.68	32.63
CSP+PCA EEG: 4-30 Hz fNIRS: 0.02-0.08 Hz	88.00±6.16	95.75±1.64	73.24
FBCSP+PCA EEG: 4~7 Hz, 8~13 Hz and 14~30 Hz fNIRS: 0.02-0.08 Hz	92.25±4.99	96.90±1.59	73.96

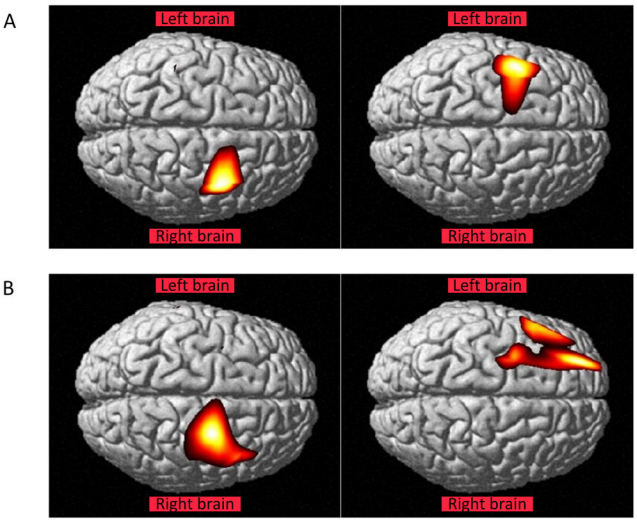

FIGURE 6. Brain activation results. A, The activation area of left-hand motor imagination and that of right-hand motor imagination in dataset A (from left to right), $p < 0.05$. B, The activation area of left-hand motor imagination and that of right-hand motor imagination in dataset B (from left to right), $p < 0.05$.

On the other hand, fMRI uses blood-oxygen-level-dependent imaging (BOLD) to detect hemodynamic processes, allowing for measurements of HbO and Hb differences based on differential magnetic susceptibility. This approach provides a relatively high spatial resolution but lower temporal resolution since it is sensitive only to the difference between two brain states. Similarly, fNIRS uses near-infrared light to estimate spectroscopic measurements of HbO and Hb variation at the cortical level. Combining EEG and fNIRS is ideal for multimodal BCIs since they are portable and require electrode caps whose density can be adjusted according to the number of leads.

In this study, the mean classification accuracy of the left-right MI was improved with simultaneous EEG-fNIRS recordings (92.25 ± 4.99%) compared to standalone EEG or fNIRS signals (EEG: 76.00 ± 8.46%, fNIRS: 71.25 ± 8.56%). Such results are in accordance with others' findings that a 5% to 24.4% improvement of BCI classification accuracy can be achieved for fused EEG-fNIRS signals in MI tasks [12], [45], [46], [47]. The main reason for the classification accuracy improvement attributes to the complementary features of these two modalities considering the volume of information, the frequency domain of signals or the spatial distribution electrodes. In addition, EEG-fNIRS-based multimodal BCI systems for other tasks also outperform those single-modal BCI systems. However, Ge et al. proposed a similar EEG-fNIRS multimodal system with fewer leads for MI classification [45]. Three EEG channels and six pairs of fNIRS channels are selected for the MI task and the mean accuracy can reach 81.2%, outperforming that with a large number of electrodes [48], [49], [50], [51]. Such a comparison implies that the redundancy of signals may contribute to the reduction of classification accuracy. To avoid feature redundancy, we applied PCA to regroup the original features with specific correlations obtained from the CSP into a new group of unrelated features and the classification accuracy can be as high as 92.25 ± 4.99%.

In addition, Chiarelli et al. also proposed an EEG-fNIRS-based multimodal BCI system for MI tasks but with a deep neural network (DNN) classifier [13]. They found the performance of the DNN classifier is better than that of an SVM one. Hemoglobin change and the event-related synchronizations/event-related desynchronizations (ERSs/ERDs) values were directly fed to DNN classifier without any preprocessing. Such a result manifests the importance of feature redundancy during the preprocessing that augments the ability of the consequent classifier.

The hybrid EEG-fNIRS BCI can also improve the classification accuracy of brain states instead of a task in a certain state albeit a limited number of channels were applied. For example, Kwon et al. proposed a hybrid EEG-fNIRS BCI system for distinguishing brain states of mental arithmetic, right-hand MI and an idle state [52]. Compared with the left-right hand MI task, telling the discrimination of brain states seems rougher and the difference is more evident as the prefrontal and parietal cortex are responsible for arithmetic tasks whereas the cerebral dorsal prefrontal cortex is responsible for left-right MI task [53], [54].

In this study, the CSP is used to extract the features from both EEG signals and fNIRS signals according to the frequency bands of EEG and the concentrations of HbO and Hb, respectively. In this way, the proportion of the fused features is deterministic and the contribution of these features to the BCI is not clear although the comparison of classification accuracy with unimodal is completed. Hosin et al. proposed a notion of fusion level of EEG/fNIRS in the multimodal BCI for MI classification. They find that the fused features with a low proportion of EEG features achieve a high level of classification accuracy which is in contradiction with our results as the classification accuracy for mere EEG signals is better than that with unimodal features of fNIRS [55]. Such a contradiction may be related to the preprocessing methods. However, making sure the proportion of features in the multimodal BCI can not only benefit the BCI design, but also it can be advantageous to the exploring of neural mechanisms in MI.

Research has found that there is an internal connection between the brain and the left and right hands, and this connection exhibits asymmetry [56]. For those who are right-handed, it is generally the left hemisphere of the brain that is used for motor performance. Some studies suggested that the asymmetry of the motor cortex may be due to right-hand preference [56], [57]. Other studies show that the left-hand movements of subjects are more affected by the visual environment without considering handedness, which strongly suggests the complex relationship between brain asymmetry and handedness [58], [59]. In fact, the motor cortex is also activated during voluntary exercise and when observing other behavior [60], [61], [62], [63], [64], [65]. Brain asymmetry is also related to the proficiency of habitual hands, which is the result of the interaction between neural connections and molecular regulation [66]. Brain asymmetry is also common in other fields, such as hemispheric asymmetry, which is used to assess the efficacy of treating depression [67]. The power spectral density topographic map of EEG also has asymmetry [68]. The motor function of the human body interacts with vision, hearing, language and memory. Therefore, the asymmetry between left and right brain regions in our activation results is the result of the interaction between the subject's left-hand and right-hand proficiency and other cognitive processes.

To demonstrate the effectiveness of our approach, we compared our results with those of other studies conducted in the past three years (Table 3). Our findings showed that the classification accuracy achieved through multimodal analysis was higher than that achieved through analysis of EEG or fNIRS signals alone [69], [70], [71], [72], [73], [74]. This could be attributed to the fact that the best results obtained from the single-mode analysis are already included in the optimal results from the multimodal analysis. Jian et al. [75] used the independent decision path fusion (IDPF) method to improve the average classification accuracy to 70.32 ± 8.74% across four types of classification problems in their EEG-fNIRS joint study. Pac et al. [77] used the pearson correlation coefficient based feature selection (PCCFS) strategy to classify EEG features derived from both EEG and fNIRS, which increased the classification accuracy from 65.52% and 58.62% achieved individually to 79.31%. Kwak et al. [78] used fNIRS to guide attention networks (FGANet), and by combining the two signals, they improved the average accuracy to 78.59 ± 8.86%. Arshia et al. [79] conducted integrated vector phase analysis (VPA) based on EEG and

TABLE 3. Comparison of research in the past three years.

Paper	Year of Publication	Mode	Method	Result
[69]	2020	EEG	Double constrained nonnegative matrix factorization (DCNMF).	Accuracy: 79.00%.
[70]	2021	EEG	End-to-end Shallow architecture.	Accuracy: 83.20%.
[71]	2022	EEG	Manifold embedded transfer learning (METL).	Accuracy: 83.14%.
[72]	2020	fNIRS	Stepwise regression analysis based on sequential feature selection (SWR-SFS) and ReliefF methods.	Accuracy:78.27%(Hb) 77.41%(HbO).
[73]	2020	fNIRS	Signal Mean (SM), Skewness (SK), Kurtosis (KR), Standard Deviation (SD), Signal Peak (SP), and Signal Variance (SV)+KNN.	Accuracy:90.54%.
[74]	2020	fNIRS	CSP+LSVM.	Accuracy:71.4%
[75]	2019	EEG+ fNIRS	Independent decision path fusion (IDPF).	Mean Accuracy:70.32±8.74%.
[76]	2020	EEG+ fNIRS	Event related potentials (ERPs) were recorded using an electroencephalogram (EEG) and oxygenated hemoglobin concentrations (Oxy-Hb) were recorded using fNIRS during a colored Go/NoGo task, simultaneously. Latencies and amplitudes of NoGo-N2 and NoGo/Go-P3 tasks were measured using EEG.	Children with ADHD showed significantly decreased Oxy-Hb in the right frontal cortex as well as longer NoGo-P3 latencies and a decreased NoGo/Go-P3 amplitude.
[77]	2020	EEG +fNIRS	Pearson correlation coefficient-based feature selection (PCCFS).	Accuracy: 79.31%.
[78]	2022	EEG+ fNIRS	fNIRS-guided attention network (FGANet).	Mean Accuracy: 78.59±8.86%
[79]	2022	EEG+ fNIRS	Vector-phase analysis (VPA).	Accuracies: 82%,89%,87% 86%.
THIS WORK	2023	EEG+fNIRS	FBCSP+PCA+SVM, GLM+MBLL.	Mean Accuracies: 92.25±4.99%. The relative activation of the left and right brain regions was significant during the exercise imagination period of the subjects.

fNIRS. The classification accuracy of support vector machine (SVM), convolutional neural network (CNN), deep neural network (DNN), and VPA (with dual threshold circles) reached 82%, 89%, 87%, and 86%, respectively. Moreover, Kaga et al. [76] used EEG to measure the latency and amplitude of NoGo-N2 and NoGo/Go-P3 tasks, and found that Oxy-HB in the right frontal cortex of children with ADHD was significantly reduced. Our brain activation study also yielded similar results, as significant changes in HbO and Hb signals were observed during motor imagery in both left- and right-brain regions. This supports the separability of our data and the reliability of our classification results.

V. CONCLUSION

In this paper, we propose a left-right hand MI decoding method based on multimodal signals. A combined preprocessing method considering CSP, FB and PCA provides high discrimination features for a SVM classifier so that the classification accuracy can reach more than 90% for both self-collected and public datasets. Such a result manifests that the combined preprocessing method can be a paradigm for multimodal BCI. In addition, we also used NIRS-SPM to show the activated areas during the MI experiment which is consistent with a large number of fMRI studies. From the perspective of activation regions, there are significant differences between left-hand and right-hand MI activation regions, which also supports our classification results from the basic neural basis of the human brain. It also shows that the premotor cortex and supplementary motor cortex, primary motor cortex play an important role in MI.

ACKNOWLEDGMENT

(Tao Xu and Zhengkang Zhou contributed equally to this work.)

REFERENCES

[1] N. Mizuguchi, H. Nakata, Y. Uchida, and K. Kanosue, "Motor imagery and sport performance," *J. Phys. Fitness Sports Med.*, vol. 1, no. 1, pp. 103–111, 2012.

[2] J. Decety and D. H. Ingvar, "Brain structures participating in mental simulation of motor behavior: A neuropsychological interpretation," *Acta Psychologica*, vol. 73, no. 1, pp. 13–34, Feb. 1990.

[3] J. Decety and J. A. Stevens, "Action representation and its role in social interaction," in *Handbook of Imagination and Mental Simulation*. Psychology Press, 2012, pp. 3–20.

[4] W. Zgallai, J. T. Brown, A. Ibrahim, F. Mahmood, K. Mohammad, M. Khalfan, M. Mohammed, M. Salem, and N. Hamood, "Deep learning AI application to an EEG driven BCI smart wheelchair," in *Proc. Adv. Sci. Eng. Technol. Int. Conf. (ASET)*, Mar. 2019, pp. 1–5.

[5] B. Xu, Z. Wei, A. Song, C. Wu, D. Zhang, W. Li, G. Xu, H. Li, and H. Zeng, "Phase synchronization information for classifying motor imagery EEG from the same limb," *IEEE Access*, vol. 7, pp. 153842–153852, 2019.

[6] K. K. Ang, K. S. G. Chua, K. S. Phua, C. Wang, Z. Y. Chin, C. W. K. Kuah, W. Low, and C. Guan, "A randomized controlled trial of EEG-based motor imagery brain–computer interface robotic rehabilitation for stroke," *Clin. EEG Neurosci.*, vol. 46, no. 4, pp. 310–320, Oct. 2015.

[7] W.-Y. Hsu and Y.-N. Sun, "EEG-based motor imagery analysis using weighted wavelet transform features," *J. Neurosci. Methods*, vol. 176, no. 2, pp. 310–318, Jan. 2009.
[8] K. K. Ang, C. Guan, K. S. G. Chua, B. T. Ang, C. W. K. Kuah, C. Wang, K. S. Phua, Z. Y. Chin, and H. Zhang, "A large clinical study on the ability of stroke patients to use an EEG-based motor imagery brain–computer interface," *Clin. EEG Neurosci.*, vol. 42, no. 4, pp. 253–258, Oct. 2011.
[9] S. H. Johnson, G. Sprehn, and A. J. Saykin, "Intact motor imagery in chronic upper limb hemiplegics: Evidence for activity-independent action representations," *J. Cognit. Neurosci.*, vol. 14, no. 6, pp. 841–852, Aug. 2002.
[10] S. H. Johnson, "Imagining the impossible: Intact motor representations in hemiplegics," *NeuroReport*, vol. 11, no. 4, pp. 729–732, Mar. 2000.
[11] A. M. Chiarelli, F. Zappasodi, F. Di Pompeo, and A. Merla, "Simultaneous functional near-infrared spectroscopy and electroencephalography for monitoring of human brain activity and oxygenation: A review," *Neurophotonics*, vol. 4, no. 4, 2017, Art. no. 041411.
[12] S. Fazli, J. Mehnert, J. Steinbrink, G. Curio, A. Villringer, K.-R. Müller, and B. Blankertz, "Enhanced performance by a hybrid NIRS–EEG brain computer interface," *NeuroImage*, vol. 59, no. 1, pp. 519–529, Jan. 2012.
[13] A. M. Chiarelli, P. Croce, A. Merla, and F. Zappasodi, "Deep learning for hybrid EEG-fNIRS brain–computer interface: Application to motor imagery classification," *J. Neural Eng.*, vol. 15, no. 3, Jun. 2018, Art. no. 036028.
[14] K.-S. Hong, N. Naseer, and Y.-H. Kim, "Classification of prefrontal and motor cortex signals for three-class fNIRS–BCI," *Neurosci. Lett.*, vol. 587, pp. 87–92, Feb. 2015.
[15] M. J. Khan, M. J. Hong, and K.-S. Hong, "Decoding of four movement directions using hybrid NIRS-EEG brain–computer interface," *Frontiers Hum. Neurosci.*, vol. 8, p. 244, Apr. 2014.
[16] A. M. Chiarelli, E. L. Maclin, K. A. Low, M. Fabiani, and G. Gratton, "Comparison of procedures for co-registering scalp-recording locations to anatomical magnetic resonance images," *J. Biomed. Opt.*, vol. 20, no. 1, 2015, Art. no. 016009.
[17] A. M. Chiarelli, E. L. Maclin, K. A. Low, K. E. Mathewson, M. Fabiani, and G. Gratton, "Combining energy and Laplacian regularization to accurately retrieve the depth of brain activity of diffuse optical tomographic data," *J. Biomed. Opt.*, vol. 21, no. 3, 2016, Art. no. 036008.
[18] D. A. Boas, C. E. Elwell, M. Ferrari, and G. Taga, "Twenty years of functional near-infrared spectroscopy: Introduction for the special issue," *NeuroImage*, vol. 85, pp. 1–5, Jan. 2014.
[19] L. Ma, L. Zhang, L. Wang, M. Xu, H. Qi, B. Wan, D. Ming, and Y. Hu, "A hybrid brain–computer interface combining the EEG and NIRS," in *Proc. IEEE Int. Conf. Virtual Environ. Hum.-Comput. Interfaces Meas. Syst. (VECIMS)*, Jul. 2012, pp. 159–162.
[20] H. Wang, C. Tang, T. Xu, T. Li, L. Xu, H. Yue, P. Chen, J. Li, and A. Bezerianos, "An approach of one-vs-rest filter bank common spatial pattern and spiking neural networks for multiple motor imagery decoding," *IEEE Access*, vol. 8, pp. 86850–86861, 2020.
[21] S. Lemm, B. Blankertz, G. Curio, and K.-R. Müller, "Spatio-spectral filters for improving the classification of single trial EEG," *IEEE Trans. Biomed. Eng.*, vol. 52, no. 9, pp. 1541–1548, Sep. 2005.
[22] G. Dornhege, B. Blankertz, M. Krauledat, F. Losch, G. Curio, and K.-R. Müller, "Combined optimization of spatial and temporal filters for improving brain–computer interfacing," *IEEE Trans. Biomed. Eng.*, vol. 53, no. 11, pp. 2274–2281, Nov. 2006.
[23] K. K. Ang, Z. Y. Chin, H. Zhang, and C. Guan, "Filter bank common spatial pattern (FBCSP) in brain–computer interface," in *Proc. IEEE Int. Joint Conf. Neural Netw., IEEE World Congr. Comput. Intell.*, Jun. 2008, pp. 2390–2397.
[24] K. P. Thomas, C. Guan, C. T. Lau, A. P. Vinod, and K. K. Ang, "A new discriminative common spatial pattern method for motor imagery brain–computer interfaces," *IEEE Trans. Biomed. Eng.*, vol. 56, no. 11, pp. 2730–2733, Nov. 2009.
[25] Y. Zhang, G. Zhou, J. Jin, X. Wang, and A. Cichocki, "Optimizing spatial patterns with sparse filter bands for motor-imagery based brain–computer interface," *J. Neurosci. Methods*, vol. 255, pp. 85–91, Nov. 2015.
[26] V. Peterson, D. Wyser, O. Lambercy, R. Spies, and R. Gassert, "A penalized time-frequency band feature selection and classification procedure for improved motor intention decoding in multichannel EEG," *J. Neural Eng.*, vol. 16, no. 1, Feb. 2019, Art. no. 016019.
[27] J. Shin, A. von Lühmann, B. Blankertz, D. Kim, J. Jeong, H. Hwang, and K. Müller, "Open access dataset for EEG+NIRS single-trial classification," *IEEE Trans. Neural Syst. Rehabil. Eng.*, vol. 25, no. 10, pp. 1735–1745, Oct. 2017.
[28] M. J. Herrmann, A. Walter, A.-C. Ehlis, and A. J. Fallgatter, "Cerebral oxygenation changes in the prefrontal cortex: Effects of age and gender," *Neurobiol. Aging*, vol. 27, no. 6, pp. 888–894, Jun. 2006.
[29] S. Ahn, T. Nguyen, H. Jang, J. G. Kim, and S. C. Jun, "Exploring neuro-physiological correlates of drivers' mental fatigue caused by sleep deprivation using simultaneous EEG, ECG, and fNIRS data," *Frontiers Hum. Neurosci.*, vol. 10, p. 219, May 2016.
[30] G. Aranyi, F. Pecune, F. Charles, C. Pelachaud, and M. Cavazza, "Affective interaction with a virtual character through an fNIRS brain–computer interface," *Frontiers Comput. Neurosci.*, vol. 10, Jul. 2016.
[31] F. Al-Shargie, M. Kiguchi, N. Badruddin, S. C. Dass, A. F. M. Hani, and T. B. Tang, "Mental stress assessment using simultaneous measurement of EEG and fNIRS," *Biomed. Opt. Exp.*, vol. 7, no. 10, pp. 3882–3898, Oct. 2016.
[32] M. Balconi and M. E. Vanutelli, "Competition in the brain. The contribution of EEG and fNIRS modulation and personality effects in social ranking," *Frontiers Psychol.*, vol. 7, p. 1587, Oct. 2016.
[33] D. Carius, C. Andrä, M. Clauß, P. Ragert, M. Bunk, and J. Mehnert, "Hemodynamic response alteration as a function of task complexity and expertise—An fNIRS study in jugglers," *Frontiers Hum. Neurosci.*, vol. 10, p. 126, Mar. 2016.
[34] L.-C. Chen, P. Sandmann, J. D. Thorne, M. G. Bleichner, and S. Debener, "Cross-modal functional reorganization of visual and auditory cortex in adult cochlear implant users identified with fNIRS," *Neural Plasticity*, vol. 2016, pp. 1–13, Oct. 2016.
[35] Y. Wang, S. Gao, and X. Gao, "Common spatial pattern method for channel selelction in motor imagery based brain–computer interface," in *Proc. Annu. Int. Conf. IEEE Eng. Med.; Biol. Soc., IEEE Eng. Med.; Biol. Soc. Conf.*, vol. 5, Jan. 2005, pp. 5392–5395.
[36] Y. Huang, J. Benesty, and G. W. Elko, "Adaptive eigenvalue decomposition algorithm for real time acoustic source localization system," in *Proc. IEEE Int. Conf. Acoust., Speech, Signal Process (ICASSP)*, vol. 2. Phoenix, AZ, USA: IEEE, Mar. 1999, pp. 937–940.
[37] Q. Ai, A. Chen, K. Chen, Q. Liu, T. Zhou, S. Xin, and Z. Ji, "Feature extraction of four-class motor imagery EEG signals based on functional brain network," *J. Neural Eng.*, vol. 16, no. 2, Apr. 2019, Art. no. 026032.
[38] I. T. Jolliffe, "Principal component analysis," *J. Marketing Res.*, vol. 87, no. 4, p. 513, 2002.
[39] S. Ali and K. A. Smith, "Matching SVM kernel's suitability to data characteristics using tree by fuzzy c-means clustering," in *Proc. 3rd Int. Conf. Hybrid Intell. Syst.*, Melbourne, VIC, Australia, Dec. 2003, pp. 553–562.
[40] L. Kocsis, P. Herman, and A. Eke, "The modified Beer–Lambert law revisited," *Phys. Med. Biol.*, vol. 51, no. 5, pp. N91–N98, Mar. 2006.
[41] J. Ye, S. Tak, K. Jang, J. Jung, and J. Jang, "NIRS-SPM: Statistical parametric mapping for near-infrared spectroscopy," *NeuroImage*, vol. 44, no. 2, pp. 428–447, Jan. 2009.
[42] A. Yazdani, T. Ebrahimi, and U. Hoffmann, "Classification of EEG signals using Dempster Shafer theory and a k-nearest neighbor classifier," in *Proc. 4th Int. IEEE/EMBS Conf. Neural Eng.* Antalya, Turkey: IEEE, Apr. 2009, pp. 327–330.
[43] E. Gerardin, A. Sirigu, S. Lehericy, J. B. Poline, B. Gaymard, C. Marsault, Y. Agid, and D. Le Bihan, "Partially overlapping neural networks for real and imagined hand movements," *Cerebral Cortex*, vol. 10, no. 11, pp. 1093–1104, 2000.
[44] L.-R. Yan, Y.-B. Wu, D.-W. Hu, S.-Z. Qin, G.-Z. Xu, X.-H. Zeng, and H. Song, "Network asymmetry of motor areas revealed by resting-state functional magnetic resonance imaging," *Behav. Brain Res.*, vol. 227, no. 1, p. 133, 2012.
[45] S. Ge, Q. Yang, R. Wang, P. Lin, J. Gao, Y. Leng, Y. Yang, and H. Wang, "A brain–computer interface based on a few-channel EEG-fNIRS bimodal system," *IEEE Access*, vol. 5, pp. 208–218, 2017.
[46] M.-H. Lee, S. Fazli, J. Mehnert, and S.-W. Lee, "Subject-dependent classification for robust idle state detection using multi-modal neuroimaging and data-fusion techniques in BCI," *Pattern Recognit.*, vol. 48, no. 8, pp. 2725–2737, Aug. 2015.
[47] H. Morioka, A. Kanemura, S. Morimoto, T. Yoshioka, S. Oba, M. Kawanabe, and S. Ishii, "Decoding spatial attention by using cortical currents estimated from electroencephalography with near-infrared spectroscopy prior information," *NeuroImage*, vol. 90, pp. 128–139, Apr. 2014.

[48] V. Kaiser, G. Bauernfeind, A. Kreilinger, T. Kaufmann, A. Kübler, C. Neuper, and G. R. Müller-Putz, "Cortical effects of user training in a motor imagery based brain–computer interface measured by fNIRS and EEG," *NeuroImage*, vol. 85, pp. 432–444, Jan. 2014.

[49] M. J. Khan, K. Hong, N. Naseer, and M. R. Bhutta, "Motor imagery performance evaluation using hybrid EEG-NIRS for BCI," in *Proc. 54th Annu. Conf. Soc. Instrum. Control Eng. Jpn. (SICE)*, Jul. 2015, pp. 1150–1155.

[50] J. Yu, K. K. Ang, C. Guan, and C. Wang, "A multimodal fNIRS and EEG-based BCI study on motor imagery and passive movement," in *Proc. 6th Int. IEEE/EMBS Conf. Neural Eng. (NER)*, Nov. 2013, pp. 5–8.

[51] R. K. Almajidy, Y. Boudria, U. G. Hofmann, W. Besio, and K. Mankodiya, "Multimodal 2D brain computer interface," in *Proc. 37th Annu. Int. Conf. IEEE Eng. Med. Biol. Soc. (EMBC)*, Aug. 2015, pp. 1067–1070.

[52] J. Kwon, J. Shin, and C.-H. Im, "Toward a compact hybrid brain–computer interface (BCI): Performance evaluation of multi-class hybrid EEG-fNIRS BCIs with limited number of channels," *PLoS ONE*, vol. 15, no. 3, Mar. 2020, Art. no. e0230491.

[53] S. M. Rivera, A. L. Reiss, M. A. Eckert, and V. Menon, "Developmental changes in mental arithmetic: Evidence for increased functional specialization in the left inferior parietal cortex," *Cerebral Cortex*, vol. 15, no. 11, pp. 1779–1790, Nov. 2005.

[54] V. Menon, S. M. Rivera, C. D. White, G. H. Glover, and A. L. Reiss, "Dissociating prefrontal and parietal cortex activation during arithmetic processing," *NeuroImage*, vol. 12, no. 4, pp. 357–365, Oct. 2000.

[55] S. M. I. Hosni, S. B. Borgheai, J. McLinden, S. Zhu, X. Huang, S. Ostadabbas, and Y. Shahriari, "A graph-based nonlinear dynamic characterization of motor imagery toward an enhanced hybrid BCI," *Neuroinformatics*, vol. 20, pp. 1–21, Jul. 2022.

[56] K. Amunts, G. Schlaug, A. Schleicher, H. Steinmetz, A. Dabringhaus, P. E. Roland, and K. Zilles, "Asymmetry in the human motor cortex and handedness," *NeuroImage*, vol. 4, no. 3, pp. 216–222, 1996.

[57] A. W. Toga and P. M. Thompson, "Mapping brain asymmetry," *Nature Rev. Neurosci.*, vol. 4, no. 1, pp. 37–48, Jan. 2003.

[58] J. J. Adam, R. Müskens, S. Hoonhorst, J. Pratt, and M. H. Fischer, "Left hand, but not right hand, reaching is sensitive to visual context," *Exp. Brain Res.*, vol. 203, pp. 227–232, Mar. 2010.

[59] C. L. R. Gonzalez, T. Ganel, and M. A. Goodale, "Hemispheric specialization for the visual control of action is independent of handedness," *J. Neurophysiol.*, vol. 95, no. 6, pp. 3496–3501, 2006.

[60] S. Caspers, K. Zilles, A. R. Laird, and S. B. Eickhoff, "ALE meta-analysis of action observation and imitation in the human brain," *NeuroImage*, vol. 50, no. 3, pp. 1148–1167, Apr. 2010.

[61] T. T.-J. Chong, R. Cunnington, M. A. Williams, N. Kanwisher, and J. B. Mattingley, "FMRI adaptation reveals mirror neurons in human inferior parietal cortex," *Current Biol.*, vol. 18, no. 20, pp. 1576–1580, Oct. 2008.

[62] V. Gazzola and C. Keysers, "The observation and execution of actions share motor and somatosensory voxels in all tested subjects: Single-subject analyses of unsmoothed fMRI data," *Cerebral Cortex*, vol. 19, no. 6, pp. 1239–1255, Jun. 2009.

[63] M.-H. Grosbras, S. Beaton, and S. B. Eickhoff, "Brain regions involved in human movement perception: A quantitative voxel-based meta-analysis," *Hum. Brain Mapping*, vol. 33, no. 2, pp. 431–454, Feb. 2012.

[64] S. Hétu, C. Mercier, F. Eugène, P.-E. Michon, and P. L. Jackson, "Modulation of brain activity during action observation: Influence of perspective, transitivity and meaningfulness," *PLoS ONE*, vol. 6, no. 9, Sep. 2011, Art. no. e24728.

[65] L. Turella, M. Erb, W. Grodd, and U. Castiello, "Visual features of an observed agent do not modulate human brain activity during action observation," *NeuroImage*, vol. 46, no. 3, pp. 844–853, Jul. 2009.

[66] T. Sun and C. A. Walsh, "Molecular approaches to brain asymmetry and handedness," *Nature Rev. Neurosci.*, vol. 7, no. 8, pp. 655–662, Aug. 2006, doi: 10.1038/nrn1930.

[67] M. A. Quraan, A. B. Protzner, Z. J. Daskalakis, P. Giacobbe, C. W. Tang, S. H. Kennedy, A. M. Lozano, and M. P. McAndrews, "EEG power asymmetry and functional connectivity as a marker of treatment effectiveness in DBS surgery for depression," *Neuropsychopharmacology*, vol. 39, no. 5, pp. 1270–1281, Apr. 2014.

[68] R. Wang, J. Wang, H. Yu, X. Wei, C. Yang, and B. Deng, "Power spectral density and coherence analysis of Alzheimer's EEG," *Cognit. Neurodynamics*, vol. 9, no. 3, pp. 291–304, Jun. 2015, doi: 10.1007/s11571-014-9325-x.

[69] J. Su, Z. Yang, W. Yan, and W. Sun, "Electroencephalogram classification in motor-imagery brain–computer interface applications based on double-constraint nonnegative matrix factorization," *Physiol. Meas.*, vol. 41, no. 7, p. 075007, 2020.

[70] D. M. Hermosilla, R. T. Codorniú, R. L. Baracaldo, R. S. Zamora, D. D. Rodriguez, Y. L. Albuerne, and J. R. N. Álvarez, "Shallow convolutional network excel for classifying motor imagery EEG in BCI applications," *IEEE Access*, vol. 9, pp. 98275–98286, 2021.

[71] Y. Cai, Q. She, J. Ji, Y. Ma, J. Zhang, and Y. Zhang, "Motor imagery EEG decoding using manifold embedded transfer learning," *J. Neurosci. Methods*, vol. 370, Mar. 2022, Art. no. 109489.

[72] E. A. Aydin, "Subject-specific feature selection for near infrared spectroscopy based brain–computer interfaces," *Comput. Methods Programs Biomed.*, vol. 195, Oct. 2020, Art. no. 105535.

[73] M. S. B. A. Ghaffar, U. S. Khan, N. Naseer, N. Rashid, and M. I. Tiwana, "Improved classification accuracy of four class FNIRS-BCI," in *Proc. 12th Int. Conf. Electron., Comput. Artif. Intell. (ECAI)*. Bucharest, Romania: IEEE, Jun. 2020, pp. 1–5.

[74] H. Kim, I. Wang, Y. Kim, H. Kim, and D. Kim, "Comparative analysis of NIRS-EEG motor imagery data using features from spatial, spectral and temporal domain," in *Proc. 8th Int. Winter Conf. Brain-Comput. Interface (BCI)*, Feb. 2020, pp. 1–4.

[75] X. Jiang, X. Gu, K. Xu, H. Ren, and W. Chen, "Independent decision path fusion for bimodal asynchronous brain–computer interface to discriminate multiclass mental states," *IEEE Access*, vol. 7, pp. 165303–165317, 2019.

[76] Y. Kaga, R. Ueda, M. Tanaka, Y. Kita, K. Suzuki, Y. Okumura, Y. Egashira, Y. Shirakawa, S. Mitsuhashi, Y. Kitamura, E. Nakagawa, Y. Yamashita, and M. Inagaki, "Executive dysfunction in medication-naïve children with ADHD: A multi-modal fNIRS and EEG study," *Brain Develop.*, vol. 42, no. 8, pp. 555–563, Sep. 2020.

[77] P. A. Cicalese, R. Li, M. B. Ahmadi, C. Wang, J. T. Francis, S. Selvaraj, P. E. Schulz, and Y. Zhang, "An EEG-fNIRS hybridization technique in the four-class classification of Alzheimer's disease," *J. Neurosci. Methods*, vol. 336, Apr. 2020, Art. no. 108618.

[78] Y. Kwak, W. Song, and S. Kim, "FGANet: FNIRS-guided attention network for hybrid EEG-fNIRS brain–computer interfaces," *IEEE Trans. Neural Syst. Rehabil. Eng.*, vol. 30, pp. 329–339, 2022.

[79] A. Arif, M. J. Khan, K. Javed, H. Sajid, S. Rubab, N. Naseer, and T. I. Khan, "Hemodynamic response detection using integrated EEG-fNIRS-VPA for BCI," *Comput., Mater. Continua*, vol. 70, no. 1, pp. 535–555, 2022.

TAO XU received the Ph.D. degree from the Department of Biomedical Engineering, City University of Hong Kong, in 2019. He joined Wuyi University as a Distinguished Professor. His research interests include computational neuroscience and neural prosthetic systems.

ZHENGKANG ZHOU was born in Hubei, China, in 1998. He received the bachelor's degree in Internet of Things engineering from the Wuchang Institute of Technology, Wuhan, China, in 2019. He is currently pursuing the master's degree in electronic information with Wuyi University, Jiangmen, China.

YULIANG YANG was born in Jiangxi, China, in 1996. He received the bachelor's degree in electrical engineering from Wuyi University, Jiangmen, China, in 2018, where he is currently pursuing the master's degree in pattern recognition and intelligent systems. He is also a member of the Jiangmen Brain-Like Computation and Hybrid Intelligence Research Center. His current research interests include brain-like computing, pattern recognition, and hybrid intelligence.

YU LI was born in Shandong, China, in 2000. He is currently pursuing the master's degree with the Faculty of Intelligent Manufacturing, Wuyi University, Jiangmen, China. He is also a member of the Jiangmen Brain-Like Computation and Hybrid Intelligence Research Center. His research interests include EEG and FNIRS signal processing and deep learning methods.

JUNHUA LI (Senior Member, IEEE) received the Ph.D. degree in computer science from the Department of Computer Science and Engineering, Shanghai Jiao Tong University, China, in 2013. He was a Senior Research Fellow with the National University of Singapore, Singapore. He is currently a Lecturer with the School of Computer Science and Electronic Engineering, University of Essex, Colchester, U.K. His research interests include computational neuroscience, brain–computer interface, machine learning, neurophysiological data analytics, and their practical applications. He is an Associate Editor of IEEE Access and a Review Editor of *Frontiers in Human Neuroscience*. He served as a guest associate editor for several special issues related to his research interests.

ANASTASIOS (TASSOS) BEZERIANOS (Senior Member, IEEE) received the Ph.D. degree in bioengineering from the University of Patras, Patras, Greece, in 1987, the degree in physics from Patras University, Patras, and the degree in telecommunication from Athens University, Athens, Greece. He is currently a Senior Researcher with the Centre for Research and Technology Hellas (CERTH), Hellenic Institute of Transport, Thessaloniki, Greece. He has been a Professor in medical physics with the Medical School, Patras University, since 2004; the Head of the Cognitive Engineering (COGEN) Laboratory, The N.1 Health Institute, National University of Singapore, Singapore, from 2012 to 2020; and a Visiting Professor with the Computer Science Department, The New South Wales University (NSWU), Canberra, ACT, Australia, from 2016 to 2020. His research interests include artificial intelligence and robotics to biomedical signal processing and brain imaging and mathematical biology and systems medicine and bioinformatics. His work is summarized in 165 journals and 240 conference proceedings publications, one book, and two patents. He has research collaborations with research institutes and universities in Japan, China, and Europe. He is a fellow of the European Alliance of Medical and Biological Engineering and Science (EAMBES) and the Founder and the Chairperson of the Biennial International Summer School on Emerging Technologies in Biomedicine and the International Workshop on Human Intelligence Machine Coexistence (HELIOS). He is also an Associate Editor of IEEE Transactions on Neural Systems and Rehabilitation Engineering (IEEE TNSRE), *Neuroscience*, and *PLOS One*. He is also a reviewer of several international scientific journals.

HONGTAO WANG (Senior Member, IEEE) received the Ph.D. degree in pattern recognition and intelligent systems from the South China University of Technology, Guangzhou, China. From 2017 to 2019, he was a Visiting Research Fellow with the National University of Singapore, Singapore. He is currently a Full Professor with the Faculty of Intelligent Manufacturing and the Deputy Director of the Discipline and Science & Technology Development Center, Wuyi University, Jiangmen, China, where he is also the Director of the Jiangmen Brain-Like Computation and Hybrid Intelligence Research Center. His current research interests include brain-like computation, pattern recognition, deep learning, and hybrid intelligence. He is an Editor of *Brain-Apparatus Communication* and has served a Guest Associate Editor for the *Frontiers in Human Neuroscience*.